Analysis of combined and isolated effects of land use and land cover changes and climate changes on the Upper Blue Nile River Basin's streamflow

5   Dagnenet Fenta Mekonnen[1,2], Zheng Duan[1], Tom Rientjes[3], Markus Disse[1]

[1]Chair of Hydrology and River Basin Management, Faculty of Civil, Geo and Environmental Engineering, Technische Universität München, Arcisstrasse 21, 80333, Munich, Germany.
[2]Amhara Regional State Water, Irrigation and Energy Development Bureau, Bahirdar, Ethiopia
[3]Department of Water Resources, Faculty of Geo-Information Science and Earth Observation (ITC), University of Twente, 10   Enschede, Netherlands
Correspondence to: Dagnenet Fenta Mekonnen (dagnfenta@yahoo.com)

Abstract: Understanding responses by changes in land use/land cover (LULC) and climate over the past decades on streamflow in the Upper Blue Nile River Basin is important for water management and water resource planning in the Nile 15   basin at large. This study assesses the long-term trends of rainfall and streamflow and analyze the responses of steamflow to changes in LULC and climate in the Upper Blue Nile River basin. Findings of the Mann-Kendal (MK) test indicate statistically insignificant increasing trends for basin-wide annual, monthly, and long rainy-season rainfall but no trend for daily, short rainy, and dry season rainfall. The Pettitt test did not detect any jump point in basin-wide rainfall series except for daily time series rainfall. Findings on MK test for daily, monthly, annual, and seasonal streamflow showed a statistically 20   significant increasing trend. Landsat satellite images for 1973, 1985, 1995, and 2010 were used for LULC change detection analysis. The LULC change detection findings indicate increases in cultivated land and decreases in forest coverage prior to 1995 but increases forest area after 1995 with area of cultivated land that diminished. Statistically, forest coverage changed from 17.4 % to 14.4 %, 12.2 %, and 15.6 % while cultivated land changed from 62.9 % to 65.6 %, 67.5 %, and 63.9 % from 1973 to 1985, in 1995, and in 2010 respectively. Results of hydrological modeling indicate that mean annual streamflow 25   increased by 16.9 % between the 1970s and 2000s due to the combined effects of LULC and climate change. Findings on effects by LULC change only on streamflow indicate that surface runoff and base flow are affected and is attributed to the 5.1 % reduction in forest coverage and 4.6 % increase in cultivated land area. Effects by climate change only revealed that the increased rainfall intensity and number of extreme rainfall events from 1971 to 2010 significantly affected the surface runoff and base flow. Hydrological impacts by climate change are more significant as compared to the impacts of LULC 30   change for streamflow of the Upper Blue Nile river basin.

1. Introduction

The Abay (Upper Blue Nile) River in Ethiopia contributes more than 60 % of the water resources in the Nile River (McCartney *et al.*, 2012). Due to the high potential of Abay river flows, the Ethiopian government conducted a series of studies since 1964 (USBR, 1964) for supporting the national development and reducing poverty (BCEOM, 1998) by increasing the number of water storage reservoirs in the Upper Blue Nile River Basin (UBNRB), both for irrigation and hydropower development. As a result, large-scale irrigation and hydropower projects such as the Grand Ethiopian Renaissance Dam (GERD), that will be the largest dam in Africa after completion, have been planned and realized along the main stem of the Blue Nile River. However, its hydrology exhibiting high seasonal flows as influenced by large variations in climate, altitude/topography, and land use/cover (LULC) change. Over the past decades, changes in climate (e.g. (Haile *et al.*, 2017)) and changes in LULC (e.g. Woldesenbet *et al.* (2017b)) have affected the magnitude of streamflow. Effective planning, management, and regulation of water resources development is therefore required to avert conflicts between the competing water users.

Only understanding the hydrological processes and sources impacting water quantity, such as LULC change and climate change, can achieve this as they are the key driving forces that can modify the watershed's hydrology and water availability (Oki and Kanae, 2006; Woldesenbet *et al.*, 2017b; Yin *et al.*, 2017b). LULC change can modify the rainfall path to generate basin runoff by altering critical water balance components, such as, groundwater recharge, infiltration, interception, and evaporation. McCartney *et al.* (2012) and Alemseged and Tom (2015) described that the UBNRB experiences significant spatial and temporal climate variability. Less than 500 mm of precipitation falls annually near the Sudanese border whereas more than 2000 mm falls annually in some areas of the southern basin (Awulachew *et al.*, 2009). Potential evapotranspiration (ET) also varies considerably and is strongly correlated with altitude. At annual bases, it varies from more than 2200 mm near the Sudanese border to between about 1300 mm and 1700 mm in the Ethiopian highlands (McCartney *et al.*, 2012). The precipitation and ET cycles are characterized by seasonal and inter-annual variability, that affect the characteristic of the UBNRB streamflow.

A literature review shows that several sub-basin or basin level studies are conducted in the UBNRB. Most of the studies were focused on trend analysis of precipitation and streamflow, for example, those by (Bewket and Sterk, 2005; Cheung *et al.*, 2008; Conway, 2000; Gebremicael *et al.*, 2013; Melesse *et al.*, 2009; Rientjes *et al.*, 2011; Seleshi and Zanke, 2004; Teferi *et al.*, 2013; Tekleab *et al.*, 2014; Tesemma *et al.*, 2010), all reported no significant trend in annual and seasonal precipitation totals within the Lake Tana sub-basin, whereas Mengistu *et al.* (2014) reported statistically non significant increasing trends in annual and seasonal rainfall series, except for a short rainy season (Belg) from February to May.

Gebremicael *et al.* (2013) reported statistically significant increasing long-term annual streamflow (1970-2005) at the El Diem gauging station for the UBNRB's streamflow. However, (Tesemma *et al.*, 2010) reported no statistically significant

trend for long term annual streamflow (1964-2003) at the El Diem gauging station, but did report a significantly increasing trend at the Bahirdar and Kessie stations. At the sub-basin scale, Rientjes *et al.* (2011) reported a decreasing trend for the low flows of Gilgel Abay sub-basin (Lake Tana catchment, the Blue Nile headwaters) during the 1973–2005 period, specifically by 18.1 % and 66.6 % in the periods 1982–2000 and 2001–2005, respectively. However, the high flows for the same periods show an increase by 7.6 % and 46.6 % due to LULC change and seasonal rainfall variability.

Although, progress has been made in assessing the impacts of LULC and climate changes on the UBNRB's hydrology, only a few studies have endeavored to assess the attribution of changes in the water balance to LULC change and climate change. Woldesenbet *et al.* (2017b), used partial least squares regression (PLSR) and a SWAT modeling approach to quantify the contributions of changes in individual LULC classes to changes in hydrological components in the Lake Tana and Beles sub-basins'. Woldesenbet *et al.* (2017b) reported that increases of cultivation land area and decreases in woody shrub/woodland appear to be major environmental stressors affecting local water resources such as increasing surface runoff and decreasing of ground water contribution in both watersheds; however, the impacts of climate change were not considered. Nonetheless, proper water resource management requires an in-depth understanding of the aggregated and disaggregated effects of LULC and climate changes on streamflow and water balance components as the interaction between LULC, climate characteristics, and the underlying hydrological processes are complex and dynamic (Yin *et al.*, 2017b).

This study's objectives are therefore to (i) assess the long-term trend of rainfall and streamflow (ii) analyze LULC change, and (iii) examining streamflow responses to the combined and isolated effects of LULC and climate changes in the UBNRB. This is doable by combining analysis of statistical trend test, change detection of LULC derived from satellite remote sensing, and hydrological modelling during the 1971–2010 period.

2. Study area

The UBNRB is located in northwestern Ethiopia. Its catchment area is about 172760 km2. Highlands, hills, valleys, and occasional rock peaks with elevations ranging from 500 m.a.s.l. to above 4000 m.a.s.l. typically characterize the basin's topography (Figure 1). According to BCEOM (1998), two thirds of the basin lies in Ethiopia's highlands with annual rainfall ranging from 800 mm to 2200 mm. The central and southeastern area is characterized by relatively high rainfall (1400 mm to 2200 mm), whereas in most of the eastern and northwestern parts of the basin rainfall is less than 1200 mm. Mekonnen and Disse (2018) showed that the UBNRB has a mean areal annual rainfall of 1452 mm and mean annual minimum and maximum temperatures of 11.4 ^{o}C and 24.7 ^{o}C, respectively.

The sub-tropical climate of the basin is affected by the movement of the Inter-Tropical Convergence Zone (ITCZ) (Conway, 2000; Mohamed et al., 2005). NMA (2013) classified the climate in Ethiopia into three distinct seasons. The main rainy

season (Kiremit) generally lasts from June to September during which southwest winds bring rains from the Atlantic Ocean. Some 70–90 % of the total rainfall occurs during this season. A dry season (Bega) lasts from October to January and the short rainy season (Belg) lasts from February to May. According to BCEOM (1998), the average annual discharge (1960 to 1992), at the Ethio-Sudan border (El Diem), is about 49.4 Billion Cubic Meter (BCM), with the low-flow month (April) equivalent to less than 2.5 % of that of the high-flow month (August). The analysis of this study revealed that the long-term (1971–2010) mean annual volume of streamflow at El Diem is 50.7 BCM, with low streamflow volume (dry season) contributing 21.1 % and the short rainy season contributing for about 6.2 %. As such some 73 % of streamflow occurred during the rainy season (Table 1). The basin's land cover essentially follows the divide between highland and lowland. Predominantly farmlands (about 90 %), bush, and shrubs cover the highlands. The lowlands, in contrast, are still largely untouched by development. As a result, woodlands, bush, and shrub lands are the dominant forms of land cover (BCEOM, 1998).

3. Input data sources

In this study, nonparametric Mann-Kendal (MK) (Kendall, 1975; Mann, 1945) statistics and the Soil and Water Assessment Tool (SWAT), developed by the Agricultural Research Service of the United States Department of Agriculture (USDA-ARS) (Arnold *et al.*, 1998), are used for statistical trend analysis and water balance modelling, respectively. Details of both methods are available in section 4. The input datasets used for the SWAT model can be categorized into those containing weather and streamflow data, and spatially distributed datasets.

3.1 Weather and streamflow data

The daily weather variables used in this study for trend analysis and for driving the water balance model are precipitation, minimum air temperature (Tmin), maximum air temperature (Tmax), relative humidity (RH), hours of sunshine (SH), and wind speed (WS). Weather data from 40 meteorological stations were obtained from the Ethiopian National Meteorological Service Agency (ENMSA) for the 1971–2010 period. Daily streamflow data for 25 gauging stations were collected from the Federal Ministry of Water, Irrigation and Electricity of Ethiopia for the same period 1971–2010. After screening and rigorous analyses of the weather data, a considerable amount of time series data were found to be missed in most of the stations (see Table S01). The occurrences of civil war, defective and outdated devices were the main causes for the missing data records. As a result, only the 15 stations (Figure 1), in which rainfall data is relatively more complete proved to be suitable for trend analysis. Some 10 stations having complete climate variables, such as Tmax, Tmin, RH, WS, and SH were used as input for the SWAT model Figure 1.

We resorted to spatial interpolation techniques, such as the inverse distance weighting (IDW), and linear regression (LR) to fill the gaps. Uhlenbrook *et al.* (2010) applied similar approaches or methods to the Gilgel Abbay sub-basin, which is the

UBNRB's headwater. The selection and number of adjacent stations for interpolation are important for the accuracy of interpolated values. As mentioned by Woldesenbet *et al.* (2017a), different authors used different criteria to select neighboring stations. Because of the relatively low number of network stations, a geographic distance of 100 km was considered for most stations when selecting neighboring stations. If no station is located within 100 km of the target station, then the search distance is increased until at least one suitable station is reached. After the neighboring stations were selected, the two methods (IDW and LR) were tested by means of cross-validation to fill in missing datasets. The candidate methods' performances were evaluated using the statistical metrics such as root mean square error (RMSE), mean absolute error (MAE), correlation coefficient (R^2), and percent bias (% bias) between observed and estimated values for the target stations. Equally weighted statistical metrics are applied to compare the performances of selected methods at target stations and to establish the ranking. A score was assigned to each candidate method according to the individual metrics. For example, the candidate achieving the smallest values of RMSE and MAE, or % bias received score 1, and score 2 for the one having larger value. The final score is obtained by summing up the score pertaining to each candidate approach at each station. The method with the smallest score is the best. The monthly, seasonal, and annual weather data were aggregated from the daily time-series data after filling the gaps. While filling in the missing data, uncertainty is expected due to low station density, poor correlations, and the considerable number of missing records. Similar techniques and approaches were used for the analysis and filling in of missing streamflow data records.

3.2 Spatial data

Spatially distributed data required for the SWAT model includes tabular and spatial soil data, tabular and spatial land use /cover information, and elevation data. A Shuttle Radar Topographic Mission Digital Elevation Model (SRTM DEM) of 90 meters' resolution from the Consultative Group on International Agricultural Research-Consortium for Spatial Information (CGIAR-CSI; http://srtm.csi.cgiar.org/SELECTION/inputCoord.asp) was used to represent land surface drainage patterns. Terrain characteristics such as slope gradient, slope length of the terrain, and stream network characteristics such as channel slope, length, and width were derived from the DEM.

The soil map (1:5000000) developed by the Food and Agriculture Organization of the United Nations (FAO-UNESCO) was downloaded from http://www.fao.org/soils-portal/soil-survey/soil-maps-and-databases/faounesco-soil-map-ofthe-world/en/. Soil information such as soil textural and physiochemical properties needed for the SWAT model were extracted from Harmonized World Soil Database v1.2, a database that combines existing regional and national soil information (http://www.fao.org/soils-portal/soil-survey/soil-maps-and-databases/harmonized-world-soil-databasev12/en/) with information provided by the FAO-UNESCO soil map (Polanco *et al.*, 2017).

The LULC maps were produced from satellite-remote-sensing Landsat images for 1973, 1985, 1995, and 2010 at a scale of 30 m x 30 m resolution. Detailed descriptions on image processing and classification are available under section 4.2.

4. Methodology

4.1 Trend analysis

The nonparametric Mann-Kendal (MK) (Kendall, 1975; Mann, 1945) statistic is chosen to detect trends for rainfall and streamflow time-series data as it is widely used for water resource planning, design, and management (Yue and Wang, 2004). Its advantage over parametric tests such as t-test is that the MK test is more suitable for non-normally distributed and missing data, which are frequently encountered in hydrological time-series (Yue *et al.*, 2004). However, the existence of positive serial correlation in time-series data affects the MK-test result. If serial correlation exists in time-series data, the MK test rejects the null hypothesis of no trend detection more often than specified by the significance level (Von Storch, 1995).

Von Storch (1995) proposed prewhitening technique to limit the influence of serial correlation on the MK test. The Effective or Equivalent Sample Size (ESS) method developed by Hamed and Rao (1998) has also been proposed to modify the variance. However, the study by (Yue *et al.*, 2002) reported that von Stroch's prewhitening is effective only when no trend exists and the ESS approach's rejection rate after modifying the variance is much higher than the actual (Yue *et al.*, 2004). Yue *et al.* (2002) then proposed trend-free prewhitening (TFPW) prior to applying the MK trend test in order to minimize it's limitation. This study therefore employed TFPW to remove the serial correlation and to detect a trend in time data series with significant serial correlation. Further details can be found in (Yue *et al.*, 2002). All the trend results in this study have been evaluated at the 5 % level of significance to ensure effective exploration of the trend..

Change point test

The Pettitt test is used to identify whether or not there is a point change or jump in the data series (Pettitt, 1979). This method detects one unknown change point by considering a sequence of random variables (Xt), X1, X2, …, XT that may have a change point at N if Xt variable for $t = 1, 2, …, N$ time step has a common distribution function, F1(x) and Xt for $t = N + 1, …, T$ time step has a common distribution function, F2(x), where $F1(x) \neq F2(x)$.

Sen's slope estimator

The trend magnitude is estimated using a nonparametric median-based slope estimator proposed by (Sen, 1968) as it is not greatly affected by gross data errors or outliers, and can be computed when data are missing. The slope estimation is given by

$$\beta = \text{Median} \left[\frac{x_j - x_k}{j - k} \right] \text{ for all } k < j, \tag{1}$$

where x_j and x_k are the sequential data values, n is the number of the recorded data. $1 < k < j < n$, and β is considered as the median of all possible combinations of pairs for the whole data set. A positive value of β indicates an upward (increasing)

trend and a negative value indicates a downward (decreasing) trend in the time series. All MK trend tests, Pettitt change-point detections, and Sen's slope analyses were conducted using the XLSTAT add-ins tool from excel (www.xlstat.com).

4.2 Remote sensing land use/cover map

4.2.1. Landsat image acquisition

5   Landsat images from the years 1973, 1985, 1995, and 2010 were accessed from the US Geological Survey (USGS) Center for Earth Resources Observation and Science (EROS) via http://glovis.usgs.gov. The Landsat images were selected based on the criteria of the acquisition period, availability, and percentage of cloud cover. Hayes and Sader (2001), recommend acquiring images from the same acquisition period to reduce image-to-image variation caused by sun angle, soil moisture, atmospheric condition, and vegetation-phenology differences. Cloud free-images were hence collected for the dry months of

10   January to May. However, as the basin covers a large area, each of the LULC map's periods comprised 16 Landsat images. Accessing all the images during a dry season in a single year was therefore difficult. Hence, images were acquired ±1 year for each time period and some images were also acquired in the months of November and December. For example, 16 Landsat MSS image scenes were acquired in 1973 (10 images in January, 4 images in December and 2 images in November; ±1 years) and merged to arrive at one LULC representation for selected years. Please see supplement Table S02 for the

15   details on Landsat images.

4.2.2 Preprocessing and processing images

Several standard preprocessing methods including geometric and radiometric correction were implemented to prepare the LULC maps from Landsat images. Although many different classification methods exist, supervised and unsupervised classifications are the two most widely used methods for landcover classification from remote-sensing images. Hence, in this

20   study, a hybrid supervised/unsupervised classification approach was adopted to classify the images from 2010 (LandsatTM). Iterative Self-Organizing Data Analysis (ISODATA) clustering was first performed to determine the image's spectral classes or land cover classes. Polygons for all of the training samples based on the identified LULC classes were then digitized using ground truth data. The samples for each land cover type were then aggregated. Finally, a supervised classification was performed using a maximum likelihood algorithm to extract four LULC classes.

A total of 488 Ground Control Points (GCPs) regarding landcover types and their spatial locations were collected from field observation in March and April 2017 using a Global Positioning System (GPS). Reference data were collected and taken from areas where there had not been any significant landcover change between 2017 and 2010. These areas were identified by interviewing local elderly people, and supplemented using high resolution Google Earth Images and the first author's

30   priori knowledge. As many as 288 GCP's were used for accuracy assessment and 200 points served as training sites to

generate a signature for each land-cover type. The classifications' accuracy was assessed by computing the error matrix (also known as the confusion matrix), which compares the classification result with ground truth information as suggested by DeFries and Chan (2000). A confusion matrix lists the values for the reference data's known cover types in the columns and for the classified data in the rows (Banko, 1998) as shown in Table 5. From the confusion matrix, a statistical metrics of overall accuracy, producers' accuracy and users' accuracy are used. Another discrete multivariate technique useful in accuracy assessment is called KAPPA (Congalton, 1991). The statistical metric for KAPPA analysis is the Kappa coefficient, which is another measure of the proportion of agreement or accuracy. The Kappa coefficient is computed as

$$K = \frac{N \sum_{i=1}^{i=r} x_{ii} \sum_{i=1}^{r}(x_{i+} * x_{+i})}{N^2 - \sum_{i=1}^{r}(x_{i+} * x_{+i})} \tag{2}$$

where r is the number of rows in the matrix, x_{ii} is the number of observations in row i and column i, x_{i+} and x_{+i} are the marginal totals of row i and column i, respectively. N is the total number of observations.

Once the landcover classification of the year 2010 Landsat image had been completed and its accuracy checked, the NDVI differencing technique (Mancino *et al.*, 2014) was applied to classify the images from 1973, 1985, and 1995. This technique was chosen to increase the accuracy of classification as it is hard to find an accurately classified digital or analog LULC map of the study area during 1973, 1985, and 1995. The information obtained from the elders is also more subjective and its reliability is questionable when there is a considerable time gap. We first calculated the NDVI from the Landsat MSS (1973) and three preprocessed Landsat TM images (1985, 1995, and 2010) following the general normalized difference between band TM4 and band TM3 images (eq. 3). The resulting successive NDVI images were subtracted from each other to assess the ΔNDVI image with positive (vegetation increase), negative (vegetation cleared) and no change at a 30 m x 30 m pixel resolution (eqs.4–6). The Landsat MSS 60 m x 60 m pixel-size data sets were resampled to a 30 m x 30 m pixel size using the "nearest neighbor" technique to have equal pixel sizes for the different images without altering the image data's original pixel values.

$$\text{NDVI} = \frac{(TM4 - TM3)}{(TM4 + TM3)} \text{ or } \frac{(MSS_3 - MSS_2)}{(MSS_3 + MSS_2)} \tag{3}$$

$$\Delta NDVI_{1995/2010} = NDVI_{1995} - NDVI_{2010} \tag{4}$$

$$\Delta NDVI_{1985/1995} = NDVI_{1985} - NDVI_{1995} \tag{5}$$

$$\Delta NDVI_{1973/1985} = NDVI_{1973} - NDVI_{1985} \tag{6}$$

The ΔNDVI image was then reclassified using a threshold value calculated as μ ± n*σ; where μ represents the ΔNDVI pixels value mean, and σ the standard deviation. The threshold identifies three ranges in the normal distribution: (a) the left tail (ΔNDVI < μ − n*σ), (b) the right tail (ΔNDVI > μ + n*σ), and (c) the central region of the normal distribution (μ − n*σ < ΔNDVI < μ + n*σ). Pixels within the two tails of the distribution are characterized by significant landcover changes, whereas pixels in the central region represent no change. To be more conservative, n = 1 was selected for this study to narrow the threshold ranges for reliable classification. The standard deviation (σ) is one of the most widely applied threshold identification approaches for different natural environments based on different remotely sensed imagery (Hu *et al.*, 2004; Jensen, 1996; Lu *et al.*, 2004; Mancino *et al.*, 2014; Singh, 1989) as cited by Mancino *et al.* (2014).

ΔNDVI pixel values (2010–1995) in the central region of the normal distribution (μ − n*σ < ΔNDVI < μ + n*σ) represent an absence of landcover change between two different periods (i.e., 1995 and 2010); therefore, pixels from 1995 corresponding to no landcover change can be classified as similar to the 2010 landcover classes. Pixels with significant NDVI change are reclassified using supervised classification, taking signatures from the already classified, no-change pixels. Likewise, 1985 and 1973 landcover images were classified based on the classified images of 1995 and 1985 respectively. Finally, after classifying the raw Landsat images into different landcover classes, change detection, which requires the comparison of independently produced classified images (Singb, 1989), was performed by the postclassification method. The postclassification change-detection comparison was conducted to determine changes in LULC between two independently classified maps from images of two different dates. Although this technique has some limitations, it is the most common approach because it does not require data normalization between two dates (Singh, 1989). This is because data from two dates are separately classified, thereby minimizing the problem of normalizing for atmospheric and sensor differences between two dates.

4.3 SWAT hydrological model

The Soil and Water Assessment Tool (SWAT) is an open-source-code, semi-distributed model with a large and growing number of model applications in a variety of studies ranging from catchment to continental scales (Allen *et al.*, 1998; Arnold *et al.*, 2012; Neitsch *et al.*, 2002). It enables the impact of LULC change and climate change on water resources to be evaluated in a basin with varying soil, land use, and management practices over a set period of time (Arnold *et al.*, 2012).

In SWAT, the watershed is divided into multiple sub-basins, which are further subdivided into hydrological response units (HRUs) consisting of homogeneous landuse management, slope, and soil characteristics (Arnold *et al.*, 1998; Arnold *et al.*, 2012). HRUs are the smallest units of the watershed in which relevant hydrologic components such as evapotranspiration,

surface runoff and peak rate of runoff, groundwater flow, and sediment yield can be estimated. Water balance is the driving force behind all of the processes in the SWAT calculated using eq. 7,

$$SW_t = SW_o + \sum_{I=1}^{t}\left(R_{day} - Q_s - Q_l - Q_b - E_a - Revap - DA\_recharge\right) \qquad (7)$$

where SW_t is the final soil-water content (mm H_2O), SW_o is the initial soil-water content on day i (mm H_2O), t is the time (days), R_{day} is the amount of precipitation on day i (mm H_2O), Q_s is the amount of surface runoff on day i (mm H_2O), Q_l is the amount of return flow on day i (mm H_2O), Q_b is the return flow from shallow aquifer on day i (mm H2O), E_a is the amount of evapotranspiration from the canopy and soil surface on day i (mm H_2O), Revap is the amount of water transferred

10   from the underlying shallow aquifer reverse upward to the soil-moisture storage on day i (mm H_2O) in response to water demand for evapotranspiration, and DA_recharge is the amount of water recharge to deep aquifer on day i (mm H_2O).

Runoff is calculated separately for each HRU and routed to obtain the total streamflow for the watershed using either the soil conservation service (SCS) curve number (CN) method (Mockus, 1964) or Green & Ampt infiltration method (GAIM)

15   (Green and Ampt, 1911), see Figure 2. However, spatial connectivity and interactions among HRUs are ignored. Instead, the cumulative output of each spatially discontinuous HRU at the sub-watershed outlet is directly routed to the channel (Pignotti *et al.*, 2017). This lack of spatial connectivity among HRUs makes implementation and impact analysis of spatially targeted management such as soil and water conservation structure difficult to incorporate into the model. Different authors have made efforts to overcome this problem for instance, a grid-based version of the SWAT model (Rathjens *et al.*, 2015) or

20   landscape simulation on a regularized grid (Rathjens and Oppelt, 2012). Moreover, (Arnold *et al.*, 2010) and (Bosch *et al.*, 2010) further modified SWAT so that it allows landscapes to be subdivided into catenas comprising upland, hillslope, and floodplain units, and flow to be routed through these catenas. However, SWATgrid, developed to overcome this limitation, remains largely untested and computationally demanding (Rathjens *et al.*, 2015).

25   Hence, the standard SWAT CN method was chosen for this study because it was applied in many Ethiopian watersheds such as (Gashaw *et al.*, 2018; Gebremicael *et al.*, 2013; Setegn *et al.*, 2008; Woldesenbet *et al.*, 2017b). Furthermore, its ability to use daily input data (Arnold *et al.*, 1998; Neitsch *et al.*, 2011; Setegn *et al.*, 2008) as compared to GAIM, which requires subdaily precipitation as a model input, and that can be difficult to obtain in data-scare regions like the UBNRB. This study focused on the effects of LULC change and climate change on the basin's water balance components, which include the

30   components of inflows, outflows, evapotranspiration, losses and the change in storage as shown in the general water balance eq. 8.

$$R = Q_t + TAE + Losses + \Delta S \qquad (8)$$

where $Q_t = Q_s + Q_l + Q_b$ and $TAE = E_c + E_s + E_t + E_r$ as it is shown in Figure 2.

R is the amount of precipitation (mm d^{-1}) as the main inflow, Qt is the total amount of streamflow (mm d^{-1}) as outflow, TAE is the total actual evapotranspiration (mm d^{-1}), E_c is evaporation from the canopy surface (mm d^{-1}), E_t is the amount of plant transpiration (mm d^{-1}), E_s is evaporation from the soil surface (mm d^{-1}) and E_r or Revap is evaporation from the shallow aquifer (mm d^{-1}) (Abiodun *et al.*, 2018), Losses are the amount of water lost from the system as a recharge to the deep aquifer (DA_recharge) (mm d^{-1}) and ΔS is the change in soil water storage (mm d^{-1}). SWAT has four storages: canopy storage (CS), soil moisture (SM), shallow aquifer (SA) and deep aquifer (DA). Water movement from the soil-moisture storage to the shallow aquifer is due to percolation, whereas water movement from the shallow aquifer reverse upward to the soil-moisture storage is Revap and water movement further from shallow aquifer to the deep aquifer is recharge. For a more detailed description of the SWAT model, refer to Neitsch *et al.* (2011).

The SWAT model setup and data preparation was done using arcSWAT2012 tool in the arcGIS environment, whereas parameter sensitivity analysis, and model calibration and validation was performed using the SWAT-CUP (Calibration and Uncertainty Procedures) interface Sequential Uncertainty Fitting (SUFI-2) algorithm (Abbaspour, 2008). During model set up, the observed daily weather and streamflow data from the given period was divided into three different periods: the first to warm up the model, the second to calibrate it, and the third to validate it. Determining the most sensitive parameters is the first step in the model calibration/validation process using the global sensitivity analysis option (Arnold *et al.*, 2012). The second step is to complete the calibration process making necessary adjustments for the model's input parameters to match model output with observed data thereby reducing the prediction uncertainty. Initial parameter estimates were taken from the default lower and upper bound values of the SWAT model database and from earlier studies in the basin such as (Gebremicael *et al.*, 2013). The final step, model validation, involves running a model using parameters that were determined during the calibration process and comparing the predictions to independently observed data not used in the calibration.

In this study, both manual and automatic calibration strategies were applied to attain the minimum differences between observed and simulated streamflows in terms of surface flow, and peak and total flow following the steps recommended by Arnold *et al.* (2012). For the purpose of impact analysis, we divided the simulation period 1971–2010 into four decadal periods hereafter referred as the 1970s (1971–1980), 1980s (1981–1990), 1990s (1991–2000) and 2000s (2001–2010) as shown in Table 2. The model's performance for the streamflow was then evaluated using statistical methods (Moriasi *et al.*, 2007) such as the Nash-Sutcliffe coefficient of efficiency (NSE), the coefficient of determination (R^2), and the relative volume error (RVE %), which are shown by eq.9-11. Furthermore, graphical comparisons of the simulated and observed data, as well as water balance checks, were used to evaluate the model's performance.

$$\mathbf{R^2} = \frac{\left[\Sigma(\mathbf{Q_{m,i}} - \bar{\mathbf{Q}}_m)(\mathbf{Q_{s,i}} - \bar{\mathbf{Q}}_s)\right]^2}{\Sigma(\mathbf{Q_{m,i}} - \bar{\mathbf{Q}}_m)^2 \Sigma \mathbf{Q_{s,i}} - \bar{\mathbf{Q}}_s^2} \qquad (9)$$

$$NSE = 1 - \frac{\Sigma(Q_{m,} - Q_s)_i^2}{(Q_{m,i} - \bar{Q}_m)^2} \qquad (10)$$

$$RVE \, (\%) = 100 * \frac{\Sigma_{i=1}^{n}(Q_m - Q_s)_i}{\Sigma_{i=1}^{n} Q_{m,i}} \qquad (11)$$

where $Q_{m,i}$ is the measured streamflow in $m^3 s^{-1}$, $\bar{Q}_m$ are the mean values of the measured streamflow ($m^3 s^{-1}$), $Q_{s,i}$ is the simulated streamflow in $m^3 s^{-1}$, and $\bar{Q}_s$ are the mean values of simulated data in $m^3 s^{-1}$.

4.4 SWAT simulations

Three different approaches were applied for assessing the effects of LULC change and climate change on streamflow and water balance components. The first approach is to assess the response of streamflow for the combined effects of LULC change and climate change. We followed the approach in (Marhaento *et al.*, 2017) and divided the analysis period, 1971–
10 2010, into four periods of similar length (four decades). These are periods when land use changes are expected to change the hydrological regime within a catchment (Marhaento *et al.*, 2017; Yin *et al.*, 2017a). The first period, the 1970s, was regarded as the baseline period. The other periods, the 1980s, 1990s, and 2000s, were regarded as altered periods. LULC maps of 1973, 1985, 1995, and 2010 were used to represent LULC patterns during the 1970s, 1980s, 1990s, and 2000s respectively. For analyses, the SWAT model was calibrated and validated for each respective period using the respective LULC map and
15 weather data (Table 2). The DEM and soil data sets remained unchanged. The differences between the simulation result of the baseline and altered periods represent the combined effects of LULC and climate changes on streamflow and water balance components

The second approach included simulations to attribute effects from LULC changes alone. It aimed to investigate whether
20 LULC change is the main driver for changes in water balance components. To identify the hydrological impacts caused solely by LULC, "A fixing-changing" method was used (Marhaento *et al.*, 2017; Woldesenbet *et al.*, 2017b; Yan *et al.*, 2013; Yin *et al.*, 2017b). The calibrated and validated SWAT model and its parameter settings in the baseline period were forced by weather data from baseline period, 1973–1980, while changing only the LULC maps from 1985, 1995, and 2010, keeping the DEM and soil data constant as suggested by (Hassaballah *et al.*, 2017b; Marhaento *et al.*, 2017; Woldesenbet *et*
25 *al.*, 2017b; Yin *et al.*, 2017b). We ran the calibrated SWAT model for the baseline period (1970s) four times changing only the LULC map for the years 1973, 1985, 1995, and 2010 and retaining the constant weather data set from the 1970s (Table 2). The third approach is similar to the second, but the simulations are attributed only for climate changes. The calibrated models for the base line period was run again four times, corresponding to the LULC periods using a unique LULC map of the year 1973 but altering the four different periods of weather data sets for respective periods.

5. Results and discussions

5.1 Trend test

5.1.1 Rainfall

The summary of the MK trend tests result for the rainfall recorded at the 15 selected stations located in and around the
UBNRB revealed a mixed trends (increasing, decreasing, and no change). For daily time series, the computed probability
values (p-values) for seven stations was greater, although for eight stations it was less, than the selected significance level (α
= 5 %). This means that no statistically significant trend existed in seven stations, but a monotonic trend occurred in the
remaining eight. Positive trends developed only at six stations, four of which were concentrated in the northern and central
highlands (Bahirdar, Dangila, Debre Markos, and G/bet). The other two stations, Assosa and Angergutten, are located in the
southwestern and southern lowlands (see Figure 1). The other two stations, Alemketema and Nedjo, which are located in the
East and Southwest of the UBNRB, respectively showed a decreasing trend. On a monthly basis, the MK trend test result
showed that no trend existed in eleven stations while statistically non significant increasing trends exist in three stations
(Dangila, G/bet and Shambu) and a decreasing trend in Alemketema station. On an annual time scale, MK trend test could
not find any trend in eleven stations but did exhibit a trend in four stations. Debiremarkos, and Shambu stations showed
statistically non significant increasing trend while G/bet and Alemketema showed statistically significant positive trend and
non significant decreasing trend respectively. The trend analysis result for the annual rainfall time series agrees well with a
previous study by Gebremicael *et al.* (2013), who reported no significant annual rainfall change at eight out of nine stations
during the 1973–2005 period. Hence, it is interesting to note that the time scale of analysis is a critical factor in determining
the given trends.

The basin-wide areal UBNRB rainfall trend and change point analysis was again carried out on daily, monthly, seasonal, and
annual time scales using the MK and Pettitt tests respectively. We applied a widely used spatial interpolation technique, the
Thiessen polygon method, to calculate basin-wide rainfall series from station data. A summary is provided in Table 3 and
Figure 3. The MK test showed increasing trends for annual, monthly, and long-rainy-season rainfall series whereas no trend
for daily, short rainy and dry-season rainfall series appeared. The magnitude of trends for annual, monthly, and long-rainy-
season rainfall series are not statistically significant, as explained by the values of Sen's slope. However, the Pettitt test could
not detect any jump point in basin-wide rainfall series except for daily time-series rainfall (see Figure S01).

Previous studies such as (Conway, 2000; Gebremicael *et al.*, 2013; Tesemma *et al.*, 2010), conducted trend analysis of basin-
wide rainfall and reported that no significant change in annual and seasonal rainfall series across the UBNRB exists, which
contradicts with the result of this study. This disagreement could be due to the number of stations and their spatial
distribution across the basin, time period of the analysis, approach used to calculate basin-wide rainfall from gauging

stations, and data sources. Tesemma *et al.* (2010) used monthly rainfall data downloaded from Global Historical Climatology Network (GHCN) data base and 10-day rainfall data for the 10 selected stations obtained from the National Meteorological Service Agency of Ethiopia from 1963–2003. Conway (2000) also constructed basin-wide annual rainfall in the UBNRB for the 1900–1998 period from the mean of 11 gauges. Furthermore, (Conway, 2000) employed simple linear

5   regressions over time to detect trends in annual rainfall series without removing the serial autocorrelation effects. Gebremicael *et al.* (2013), used only nine stations from the 1970–2005 period. However, in this study, we used daily observed rainfall data from 15 stations collected from Ethiopian Meteorological Agency from 1971–2010. The stations are more or less evenly distributed over the UBNRB.

5.1.2 Streamflow

10   The MK test's result for daily, monthly, annual, and seasonal (long and short rainy season and dry season) streamflow time series showed a positive trend, the magnitude of which is statistically significant, as summarized in Table 3 . The Pettitt test also detected change point for daily, annual, and short-rainy-season streamflow but did not detect change point for monthly, long, and dry season streamflow (see Figure 3 and Figure S02). The change point detected by the Pettitt test for annual streamflow is in 1995 whereas for daily and short rainy seasons it is in 1985 and 1987, respectively. The result obtained from

15   the MK test agrees well with the findings in Gebremicael *et al.* (2013), who reported an increasing trend in the observed annual, short, and long rain seasons' streamflow at the El Diem gauging station, but our results disagree to findings for dry-season streamflow. Furthermore, the increasing trend of long-rainy-season streamflow agrees well with the result of Tesemma et al. (2010), but disagrees with the results of short rainy season and annual flows. (Tesemma *et al.*, 2010), reported that the short rainy season and the annual flows are constant for the 1964–2003 period. This disagreement is likely

20   attributable to the difference in analysis period, as can be seen from Figure 3. The last seven years, 2004–2010, had relatively higher streamflow records.

Although, the results of the MK test for annual and long-rainy-season rainfall and streamflow show an increasing trend for the last 40 years in the UBNRB, the magnitude of Sen's slope for streamflow is much greater than it is for rainfall (Table 3).

25   Moreover, short-rainy-season streamflow shows a statistically significant positive increase whereas the rainfall shows no change. The mismatch between rainfall and streamflow trend magnitude could be associated with evapotranspiration and attributable to the combined effect of LULC change and climate change, infiltration rate due to changing soil properties, rainfall intensity, and extreme events.

5.2 LULC change analysis

30   According to the confusion-matrix report, overall accuracy of 80 %, producer's accuracy values for all classes ranged from 75.4 % to 100 %, user's accuracy values ranging from 83.7 % to 91.7 % and a kappa coefficient (k) of 0.77 were attained for

the 2010 classified image (Table 5). Monserud (1990) suggested a kappa value of <40 % as poor, 40–55 % fair, 55–70 % good, 70–85 % very good, and >85 % as excellent. According to these ranges, the classification in this study has very good agreement with the validation data set and meets the minimum accuracy requirements to be used for further change detection and impact analysis.

The classified images of the basin (Figure 4) have shown different LULC proportions at four distinct time periods, as shown in Figure 5. Cultivated land dominantly covers (62.9 %) of UBNRB, followed by bushes and shrubs (18 %), forest (17.4 %), and water (1.74 %) in 1973. In 1985, cultivated land area increased to 65.6 %, followed by bushes and shrubs (18.3 %), while forest decreased to 14.4 %, and water remained unchanged at 1.7 %. In 1995, cultivated land area further increased to
10 67.5 %, followed by bushes and shrubs (18.5 %). Forest further decreased to 12.2 % and water remained unchanged at 1.7 %. In 2010, cultivated land decreased to 63.9 %, bushes and shrubs increased to 18.8 %, forest increased to 15.6 %, and water remained unchanged at 1.7 %. During the entire 1973–2010 period, cultivated land, along with bushes and shrubs remained the major proportions compared to the other LULC classes. The highest increase (2.7 %) and the largest decrease (−3.6 %) in cultivated land occurred during the 1973–1985 and 1995–2010 periods respectively. The largest increase in
15 bushes and shrubs was 0.3 % from 1973 to 1985, whereas the largest increase in forest coverage (3.4 %) was recorded during the 1995–2010 period. Water coverage remained unchanged from 1973 to 2010.

Although, the image classification results show very good accuracy, uncertainties in classification could be expected. First, as elsewhere in Ethiopia, LULC may change rapidly over the land surface of the basin and image reflectance may be
20 confusing due to the topography and variation in the image acquisition date. Landsat images were not all available for one particular year or one season (as described under section 4.2.1); images from different years and different seasons might harbor errors. Secondly, the workflow associated with LULC classification involves many steps and can be a source of uncertainty. The errors are observed in the classified LULC map as shown in Figure 4. On the western side of the map in Figure 4 (a) a rectangular section with forest appears, that completely disappears in 4(b). Rectangular forest cover appears in
25 the northern part of the country in 4(b), which again disappears completely in 4(c). In 4(d), forest cover with linear edges (North-South) appears on the map's eastern side. That being recognized, the land-cover mapping is reasonably accurate overall, providing a good base for land-cover estimation and for providing basic information for the hydrological impact analysis.

30 The rate of expansion of cultivated land before 1995 was higher than after 1995. Conversely, the area of the forest land decreased in 1985 and 1995 with reference to the 1973 baseline. However, after 1995, the forest's size increased again whereas cultivated land decreased. The increased forest coverage and the decrease in cultivated land over the period 1995 to 2010 showed that the environment was recovering from the devastating drought, and forest clearing for firewood and cultivation due to population growth has been minimized. This could be due to the afforestation program, which the

Ethiopian government initiated, and to the extensive soil and water conservation measures carried out by the community. Since 1995, eucalyptus tree plantation expanded significantly across the country at homestead level for fire wood, construction material, charcoal production, and income generation (Woldesenbet *et al.*, 2017b). In summary, forest coverage decreased by 1.8 %, while both bushes and shrubs as well as cultivated land increased by 0.8 % and 1 % respectively during
5   the 2010 period from the original 1973 level. This result agrees well with other studies (Gebremicael *et al.*, 2013; Rientjes *et al.*, 2011; Teferi *et al.*, 2013; Woldesenbet *et al.*, 2017b), who reported a significant conversion of natural vegetation cover into agricultural land.

5.3 SWAT model calibration and validation

10   The SWAT model's most sensitive parameters for simulating streamflow were identified using global sensitivity analysis of SWAT-CUP. Their optimized values were determined by the calibration process that Arnold *et al.* (2012) recommended. Parameters such as SCS curve number (CN2), base flow alpha factor (ALPHA_BF), soil evaporation compensation factor (ESCO), threshold water depth in the shallow aquifer required for return flow to occur (GWQMN), groundwater "revap" coefficient (GW_REVAP), and available water capacity (SOL_AWC) were found to be the most sensitive parameters for the
15   streamflow predictions.

Figure 6 shows the calibration and the validation results for monthly streamflow hydrographs for each models. These results revealed that the model represents the monthly hydrographs well as also indicated by R^2, NSE, and RVE (%) statistical performance measures (Table 6). For the calibration period, the values of R^2, NSE, and RVE (%) range from 0.79 to 0.91,
20   0.74 to 0.91, and −3.4 % to 4 %, respectively. For the validation period they ranged from 0.84 to 0.94, 0.82 to 0.92 and −7.5 % to 7.2 % respectively. According to the rating of Moriasi *et al.* (2007), the SWAT model's performance over the UBNRB can be categorized as very good, although underestimation was observed in the baseflow simulation. The optimal parameter values of the four calibrated-model runs are shown in Table 7. A change was obtained for CN2 parameter values, which can be attributed to the catchment's response behavior. For instance, an increase in the absolute average (basin-wide) CN2 value
25   in the 1980s and 1990s from 72.9 to 74.7 and 75.6 compared to the 1970s respectively, indicate a reduction in forest coverage and expansion of cultivated land. On the contrary, a decrease in CN2 value was attained during the period 1990s to 2000s from 75.6 to 73.6, attributed to the increase in forest coverage and reduction in cultivated land.

5.4 Combined effects of LULC change and climate change on streamflow and water balance components

The simulation results of the four independent, decadal-time-scale calibrated and validated SWAT model runs reflect the
30   combined effect of both LULC and climate change during the past 40 years (Table 8). From the simulation result, mean annual streamflow increased by 16.9 % between the 1970s and the 2000s, while the observed mean annual streamflow

increased by 15.3 % for the same period. However, the rate of change is different in different decades. For example, it increased by 3.4 % and 9.9 % during the 1980s and 1990s respectively from the baseline 1970s period.

The ratio of mean annual streamflow to mean annual precipitation (Qt/P) increased from 19.4 % to 22.1 % while the actual
5 evaporation to precipitation (Ea/P) ratio decreased from 61.1 % to 60.5 % from the 1970s to 2000s. Moreover, the ratio of surface runoff to streamflow (Qs/Qt) increased notably from 40.7 % in the 1970s to 50.1 % and 55.4 % in the 1980s and 1990s respectively, and decreased to 43.7 % in the 2000s. In contrast, the base flow to streamflow ratio (Qb/Qt) notably decreased from 17.1 % in the 1970s to 10.3 % and 3.2 % respectively during the 1980s and 1990s, but has increased to 20 % in the 2000s. The result for surface runoff agrees to findings in (Gebremicael *et al.*, 2013), but disagreement is observed for
10 baseflow. The study reported that surface runoff (Qs) contribution to the total river discharge increased by 75 %, while the baseflow (Qb) decreased by 50 % from the 1970s to 2000s.

In general, 1.8 % forest cover loss and 1 % increased cultivated land combined with 2.2 % increased rainfall from the 1970s to the 2000s led to a 16.9 % increase in simulated streamflow. The 1990s was the period during which the greatest
15 deforestation and expansion of cultivated land was reported; meanwhile, it is the time when the rainfall intensity and the number of rainfall events have significantly increased compared to the 1970s and 1980s, as shown in Table 4. Hence, the increased mean annual streamflow could be ascribed to the combined effects of LULC and climate change. In the case of (Qs/Qt), the increasing pattern could be ascribed to increasing rainfall intensities and the expansion of cultivated land and diminution of forest coverage, which might adversely affect soil/water storage and decrease rainfall infiltration, thereby
20 increasing water yield or streamflow. In contrast, the decreasing Qb/Qt is positively related to the increasing evapotranspiration linked to both LULC and climate factors (Table 8). This hypothesis can be explained with the change in CN2 parameter values obtained during calibration of the four SWAT model runs. The CN2 parameter value which is a function of evapotranspiration derived from LULC, soil type, and slope increased in the 1980s and 1990s relative to the 1970s, and could be associated with the expansion of cultivated land and shrinkage of forest land. The increasing CN2
25 results reflect more surface runoff and less baseflow being generated.

Another important factor contributing to decreasing of surface runoff and increasing base flow ratio from 1990s to the 2000s could be the establishment of soil and water conservation (SWC) measures. According to Haregeweyn *et al.* (2015), various nationwide SWC initiatives such as Food for Work (FFW), Managing Environmental Resources to Enable Transition
30 (MERET) to more sustainable livelihoods, Productive Safety Net Programs (PSNP), Community Mobilization through free-labor days, and the National Sustainable Land Management Project (SLMP) have been undertaken since the 1980s. Haregeweyn *et al.* (2015) evaluated these initiatives' effectiveness and concluded that community labor mobilization seems to be the best approach. This can reduce mean seasonal surface runoff by 40 %, with broad spatial variability ranging from 4 % in Andit Tid (northwest Ethiopia) to 62 % in Gununo (south Ethiopia).

5.5 Effects of an isolated LULC change on streamflow and water balance components

(Yan *et al.*, 2013) used "A fixing -changing" method, which was also applied to this study, to identify the hydrological impacts of LULC change alone. The calibrated and validated SWAT model and its parameter settings in the baseline period was forced by weather data from the baseline 1973–1980 period while changing only the LULC maps from 1985, 1995, and 2010, keeping the DEM and soil data constant as suggested by Hassaballah *et al.* (2017a). The result from Figure 7 indicated that Q_s/Q_t ratio changed from 40.7 % to 41.2 %, 41.9 %, and 40.9 % respectively by using the LULC maps from 1973, 1985, 1995 and 2010, whereas the Q_b/Q_t ratio changed from 17.1 % to 16.8 %, 16.5 %, and 16.9 % respectively. The largest Q_s/Q_t ratio (41.9 %) and the smallest Q_b/Q_t ratio (16.5 %) were recorded with the 1995 LULC map. This could be attributed to the 5.1 % reduction in forest coverage and 4.6 % increase in cultivated land with the 1995 LULC map relative to the 1973 LULC map.

On a basin scale over a decadal time period, water gains mainly from precipitation. The losses are mainly due to runoff and evapotranspiration (Oki *et al.*, 2006) as the losses due to the deep percolation over the whole UBNRB is negligible (Steenhuis *et al.*, 2009). The long term mean annual deep percolation simulated in this study is about 16.7 mm constant in four decadal periods, which is about 6 % of the total water yield. With the fixing-changing approach, the change in streamflow attributable to LULC change was essentially the change in evapotranspiration between the two periods, as the amount of precipitation was constant (1970s) and the change in water storage during the two periods was similar (Yan *et al.*, 2013). Annual E_a losses from seasonal crops are smaller than those from forests, because seasonal crops transpire during a relatively shorter time interval than perennial trees do (Yan *et al.*, 2013). As a result, the actual mean annual E_a simulated by the SWAT model was 871.6 mm at the baseline. It decreased to 871.4 mm and 871 mm in 1985 and 1995 respectively and increased to 872.1 mm in 2010. This could be due to simultaneous expansion of cultivated land and shrinkage in forest coverage in the 1985 and 1995 LULC maps relative to the 1973 base line. Furthermore, this deforestation may reduce canopy interception of the rainfall, decrease soil infiltration by increasing raindrop impacts, and reducing plant transpiration, which can significantly increase surface runoff and reducing base flow (Huang *et al.*, 2013). Here, the evapotranspiration change caused by the LULC change is minimal. As a result, the change for surface runoff and baseflow is not significant.

5.6 Effects of isolated climate change on streamflow and water balance components

The impacts of climate change are analyzed by running the four models using a unique LULC map from 1973 with its model parameters while changing only the weather data sets from 1970s, 1980s, 1990s, and 2000s. The simulated water balance components shown in Figure 7 indicate that the Q_s/Q_t ratio increased from 40.7 % to 45.2 %, 45.6 %, and 46.2 % during the 1970s, 1980s, 1990s and 2000s respectively, while the Q_b/Q_t ratio changed from 17.1 % to 13.5 %, 14.9 %, and 12.7 % for the same simulation periods. The decreasing Q_b/Q_t ratio for the altered periods compared to the baseline period could be attributed to evapotranspiration changing from 872 mm to 854 mm, 906 mm, and 884 mm respectively in 1970s, 1980s,

1990s, and 2000s, which can be linked to temperature and amount of rainfall. However, it is important to know the dominant rainfall-runoff process in the study area to fully understand the effect of climate change on the water balance components.

Although, no detailed research has been conducted on the Upper Blue Nile basin to investigate the runoff-generation processes, Liu *et al.* (2008) investigated the rainfall-runoff processes at three small watersheds located inside and around the Upper Blue Nile basin, namely, Mayber, AnditTid, and Anjeni. Their analysis showed that, unlike in temperate watersheds, in monsoonal climates, a given rainfall volume at the onset of the monsoon produces a different runoff volume than the same rainfall at the end of the monsoon. Liu *et al.* (2008) and Steenhuis *et al.* (2009) showed that the ratio of discharge to precipitation minus evapotranspiration, Q/(P − ET), increases with cumulative precipitation from the onset of monsoon. This suggests that saturation excess processes play an important role in watershed response.

Furthermore, the infiltration rates that Engda (2009) measured in 2008 were compared with rainfall intensities in the Maybar and Andit Tid watersheds located inside and around the UBNRB. In the Andit Tid watershed, which has an area of less than 500 ha, the measured infiltration rates at 10 locations were compared with rainfall intensities considered from the 1986 – 2004 period. The analysis showed that only 7.8 % of rainfall intensities were found to be higher than the lowest soil infiltration rate of 25mm h^{-1}. Derib (2005) performed a similar analysis in the Maybar watershed (with a catchment area of 113 ha). The infiltration rates measured from 16 measurements ranged from 19 mm h^{-1} to 600 mm h^{-1} with a 240 mm h^{-1} average and 180 mm h^{-1} median whereas the average daily rainfall intensity from 1996 to 2004 was 8.5 mm hr^{-1}. Hence, he suggested from these infiltration measurements that infiltration excess runoff is not a common feature in these watersheds.

From the above discussion points, it is to be noted that surface runoff could increase with increasing total rainfall amount regardless of rainfall intensity. However, the mean annual rainfall amount in this study was decreasing from the 1970s to the 1980s (1428 mm and 1397 mm respectively) while the (Qs/Qt) ratio increased from 40.7 % to 45.2 %. Similarly, the mean annual rainfall amount in the 1990s (1522 mm) was greater than the mean annual rainfall amount in the 2000s (1462 mm) while the (Qs/Qt) increased from 45.6 % to 46.2 %. In contrast, climate indexes such as 99-percentile rainfall, SDII (ratio of total precipitation amount to number of days when rainfall >1 mm (R1mm)), and number of days when rainfall >20 mm (R20mm) increase consistently from 1970 to the 2000s, as shown in Table 4. This indicates that the increasing of surface runoff might be due to an increasing of number of extreme rainfall events and rainfall intensity. Although, we did not use hourly rainfall data for the SWAT model, this study suggested that infiltration excess of overland flow dominates the rainfall-runoff processes in the UBNRB, not saturation excess of overland flow. The contradiction from the previous studies might be due either to the limitation of the SWAT- CN method when applied in monsoonal climates or the overlooked of tillage activities, which significantly impact the soil infiltration rate. Extensive tillage activities are carried out across the basin at the beginning of the rainy season. Soils get disturbed as a result, which can increase the infiltration rate and ultimately decrease the amount of rainfall converted to runoff.

Although the CN method is easy to use and provides acceptable results for discharge at the watershed outlet in many cases, researchers have concerns about its use in watershed models (Steenhuis *et al.*, 1995; White *et al.*, 2011). The SWAT-CN model relies with a statistical relationship between soil moisture condition and CN value obtained from plot data in the United States with a temperate climate that was never tested in a monsoonal climate exhibiting two extreme soil moisture conditions. In monsoonal climates, long periods of rain can lead to prolonged soil saturation whereas during the dry period, the soil dries out completely, which may not happen in temperate climates (Steenhuis *et al.*, 2009). Hence, further research that considers bio-physical activities such as tillage and seasonal effects on soil moisture at representative watersheds of the basin is necessary to properly assess the rainfall-runoff processes.

6. Conclusions

This study's objectives were to understand the long-term variations of rainfall and streamflow in the UBNRB using statistical techniques (MK and Pettitt tests), and to assess the combined and isolated effects of climate and LULC change using a semi-distributed hydrological model (SWAT). Although the results of the MK test for annual and long-rainy-season rainfall and streamflow show an increasing trend over the last 40 years, the magnitude of Sen's slope for streamflow is much larger than the Sen's slope of areal rainfall. Moreover, for the short-rainy-season streamflow shows a statistically significant positive increase while the rainfall shows no change. The mismatch of trend magnitude between rainfall and streamflow could be attributed to the combined effect of LULC and climate change, associated with decreasing actual evapotranspiration (Ea) and increasing rainfall intensity and extreme events.

LULC change detection was assessed by comparing the classified images. The result showed that the dominant process is largely the expansion of cultivated land and decrease in forest coverage. The rate of deforestation is high during the 1973–1995 period. This is probably due to the severe drought that occurred in the mid-1980s and to a large population increase resulting from the expansion of agricultural land. On the other hand, forest coverage increased by 3.4 % during the period 1995 to 2010. This indicates that the environment was recovering from the devastating drought in the 1980s, regenerating of forests as the result of afforestation program initiated by the Ethiopian government, and due to soil and water conservation activities accomplished by the communities.

The SWAT model was used to analyze the combined and isolated effects of LULC and climate changes on the monthly streamflow at the basin outlet (El Diem station, located on the Ethiopia-Sudan border). The result showed that the combined effects of the LULC and climate changes increased the mean annual streamflow by 16.9 % from the 1970s to the 2000s. The increased mean annual streamflow could be ascribed to the combined effects of LULC and climate change. The LULC change alters the catchment responses. As a result, SWAT model parameter values could be changed. For instance, the

expansion of cultivation land and the shrinkage of forest coverage from 1973 to 1995 changed the basin average CN2 parameter values from 72.9 in 1973 to 74.7 and 75.6 in 1985 and 1995 respectively. Increasing of CN2 value might increase surface runoff and decrease base flow. Similarly, the increase in rainfall intensity and extreme precipitation events led to a substantial increase in Qs/Qt, a substantial decrease in Qb/Qt, and ultimately to increases in the streamflow during the 1971–2010 simulation period.

The "fixing-changing" approach result using the SWAT model revealed that the isolated effect of LULC change could potentially alter the streamflow generation processes. The result from Figure 7 shows that surface runoff is increasing while baseflow is decreasing due to expansion of cultivated land and reduction of forest coverage that reduce evapotranspiration during the periods 1985 and 1995 as compared to the baseline period 1973 LULC map. Furthermore, the SWAT simulation result from Table 8 and Figure 7 revealed that the Revap is a significant contributor to the TAE in the UBNRB for the last 40 years, with mean annual contribution ranged from 21.4–25.6 %, this could be due to the large coverage of deep rooted Eucalyptus tree species that can access the saturated zone (Neitsch *et al.*, 2011). The Revap component in this study appears consistent with the results of (Abiodun *et al.*, 2018; Benyon *et al.*, 2006), who reported the annual groundwater ET contribution to total ET ranged from 13–72 % and 20 % respectively for south-eastern Australia and Sixth Creek Catchments. However, detail investigation for the contribution of depth to water table for Revap in the study area is required which is beyond the scope of this study. In general, a 5.1 % reduction in forest coverage and a 4.6 % increase in cultivated land led to a 9.9 % increase in mean annual streamflow from 1973 to 1995. This study provides a better understanding and substantial information about how climate and LULC change affects streamflow and water balance components separately and jointly, which is useful for basin-wide water resources management. The SWAT simulation indicated that the impacts of climate change are more substantial than the impacts of LULC change, as shown in Figure 7. Surface water is no longer used for agriculture and plant consumption in areas such as the UBNRB, where water-storage facilities are scarce. On the other hand, base flow provides the most reliable source for the irrigation needed to increase agricultural production. Hence, the increasing amount of surface water and diminished base flow caused by both LULC and climate changes negatively affect socio-economic developments in the basin.

Protecting and conserving the natural forests and expanding soil-and-water conservation activities is therefore highly recommended, not only to increase the base flow available for irrigation but also to reduce soil erosion. Doing so might increase productivity, and improve the livelihoods and regional-water-resource-use cooperation. However, the uncertainties of Landsat image classification and the model uncertainty of SWAT simulation might limit this study. To improve the accuracy of LULC classification from Landsat images, further efforts such as integrating other images with Landsat images through image-fusion techniques (Ghassemian, 2016) are required. The SWAT model does not adjust CN2 for slopes greater than 5%. This could be significant in areas where the majority of the area has a slope greater than 5%, such as in the UBNRB. We therefore suggest adjusting CN2 values for slope >5 % outside of the SWAT model might improve the results.

Moreover, further research involving rainfall intensity, infiltration rate, and event-based analysis of hydrographs and critical evaluation of rainfall-runoff processes in the study area might overcome this study's limitations. Finally, the authors would like to point out that the impacts of current and future water resource developments should be investigated to establish comprehensive, holistic water resource management in the Nile basin.

Data availability. The data can be made available upon request to the corresponding author.

Competing interests. The authors declare that they have no conflict of interest.

Acknowledgements. The authors would like to thank the Ethiopian Ministry of Water, Irrigation and Electricity and the Ethiopian National Meteorological Services Agency for providing the streamflow and meteorological data, respectively. The first author received financial support from the DAAD water-food-energy NeXus project. for free. The authors would also like to express their gratitude to the anonymous referees and the editor, Prof. Axel Bronstert, who gave constructive remarks and comments for enhancing the quality of the manuscript.

References

Abbaspour, C.K.: SWAT Calibrating and Uncertainty Programs. A User Manual. Eawag Zurich, Switzerland, 2008.

Abiodun, O.O., Guan, H., Post, V.E., Batelaan, O.: Comparison of MODIS and SWAT evapotranspiration over a complex terrain at different spatial scales. Hydrology and Earth System Sciences, 22(5), 2775-2794, 2018. DOI:10.5194/hess-22-2775-2018

Alemseged, T.H., Tom, R.: Evaluation of regional climate model simulations of rainfall over the Upper Blue Nile basin. Atmospheric research, 161, 57-64, 2015. DOI:10.1016/j.atmosres.2015.03.013

Allen, R.G., Pereira, L.S., Raes, D., Smith, M.: Crop evapotranspiration-Guidelines for computing crop water requirements-FAO Irrigation and drainage paper 56. FAO, Rome, 300(9), D05109, 1998.

Arnold, J.G., Srinivasan, R., Muttiah, R.S., Williams, J.R.: Large area hydrologic modeling and assessment part I: Model development1. Wiley Online Library, 1998. DOI:10.1111/j.1752-1688.1998.tb05961.x

Arnold, J.G., Allen, P., Volk, M., Williams, J., Bosch, D.: Assessment of different representations of spatial variability on SWAT model performance. Transactions of the ASABE, 53(5), 1433-1443, 2010.

Arnold, J.G., Moriasi, D.N., Gassman, P.W., Abbaspour, K.C., White, M.J., Srinivasan, R., Santhi, C., Harmel, R., Van Griensven, A., Van Liew, M.W.: SWAT: Model use, calibration, and validation. Transactions of the ASABE, 55(4), 1491-1508, 2012.

Awulachew, S.B., McCartney, M., Steenhuis, T.S., Ahmed, A.A.: A review of hydrology, sediment and water resource use in the Blue Nile Basin, 131. IWMI, 2009.

Banko, G.: A review of assessing the accuracy of classifications of remotely sensed data and of methods including remote sensing data in forest inventory IASA Interim Report. IIASA, Laxenburg, Austria, IR-98-08, 1998.

BCEOM: Abbay river basin integrated development master plan project, phase 3 main report. Ministry of Water Resources, Addis Ababa, Ethiopia, Volume I, Main report, 1998.

Benyon, R.G., Theiveyanathan, S., Doody, T.M.: Impacts of tree plantations on groundwater in south-eastern Australia. Australian Journal of Botany, 54(2), 181-192, 2006. DOI:10.1071/BT05046

5 Bewket, W., Sterk, G.: Dynamics in land cover and its effect on stream flow in the Chemoga watershed, Blue Nile basin, Ethiopia. Hydrological Processes, 19(2), 445-458, 2005. DOI:10.1002/hyp.5542

Bosch, D., Arnold, J., Volk, M., Allen, P.: Simulation of a low-gradient coastal plain watershed using the SWAT landscape model. Transactions of the ASABE, 53(5), 1445-1456, 2010.

Cheung, W.H., Senay, G.B., Singh, A.: Trends and spatial distribution of annual and seasonal rainfall in Ethiopia. 10 International Journal of Climatology, 28(13), 1723-1734, 2008. DOI:10.1002/joc.1623

Congalton, R.G.: A review of assessing the accuracy of classifications of remotely sensed data. Remote sensing of environment, 37(1), 35-46, 1991.

Conway, D.: The climate and hydrology of the Upper Blue Nile River. The Geographical Journal, 166(1), 49-62, 2000.

15 DeFries, R., Chan, J.C.-W.: Multiple criteria for evaluating machine learning algorithms for land cover classification from satellite data. Remote Sensing of Environment, 74(3), 503-515, 2000.

Derib, S.D.: Rainfall-runoff processes at a hill-slope watershed: case of simple models evaluation at Kori-Sheleko Catchments of Wollo, Ethiopia, M. Sc. Thesis, 2005.

Engda, T.A.: Modeling rainfall, runoff and soil loss relationships in the northeastern highlands of Ethiopia, andit 20 tid watershed, Citeseer, 2009.

Gashaw, T., Tulu, T., Argaw, M., Worqlul, A.W.: Modeling the hydrological impacts of land use/land cover changes in the Andassa watershed, Blue Nile Basin, Ethiopia. Science of The Total Environment, 619, 1394-1408, 2018. DOI:10.1016/j.scitotenv.2017.11.191

Gebremicael, T., Mohamed, Y., Betrie, G., van der Zaag, P., Teferi, E.: Trend analysis of runoff and sediment 25 fluxes in the Upper Blue Nile basin: A combined analysis of statistical tests, physically-based models and landuse maps. Journal of Hydrology, 482, 57-68, 2013. DOI:10.1016/j.jhydrol.2012.12.023

Ghassemian, H.: A review of remote sensing image fusion methods. Information Fusion, 32, 75-89, 2016. DOI:10.1016/j.inffus.2016.03.003

Green, W.H., Ampt, G.: Studies on Soil Phyics. The Journal of Agricultural Science, 4(01), 1-24, 1911.

30 Haile, A.T., Akawka, A.L., Berhanu, B., Rientjes, T.: Changes in water availability in the Upper Blue Nile basin under the representative concentration pathways scenario. Hydrological sciences journal, 62(13), 2139-2149, 2017. DOI:10.1080/02626667.2017.1365149

Hamed, K.H., Rao, A.R.: A modified Mann-Kendall trend test for autocorrelated data. Journal of Hydrology, 204(1-4), 182-196, 1998.

35 Haregeweyn, N., Tsunekawa, A., Nyssen, J., Poesen, J., Tsubo, M., Tsegaye Meshesha, D., Schütt, B., Adgo, E., Tegegne, F.: Soil erosion and conservation in Ethiopia: a review. Progress in Physical Geography, 39(6), 750-774, 2015. DOI:10.1177/0309133315598725

Hassaballah, K., Mohamed, Y., Uhlenbrook, S., Biro, K.: Analysis of streamflow response to land use and land cover changes using satellite data and hydrological modelling: case study of Dinder and Rahad 40 tributaries of the Blue Nile (Ethiopia–Sudan). Hydrology and Earth System Sciences, 21(10), 5217, 2017a. DOI:10.5194/hess-21-5217-2017

~~Hassaballah, K., Mohamed, Y., Uhlenbrook, S., Biro, K.: Analysis of streamflow response to land use land cover changes using satellite data and hydrological modelling: case study of Dinder and Rahad tributaries of the Blue Nile (Ethiopia/Sudan). 2017b.~~

Hayes, D.J., Sader, S.A.: Comparison of change-detection techniques for monitoring tropical forest clearing and vegetation regrowth in a time series. Photogrammetric engineering and remote sensing, 67(9), 1067-1075, 2001.

Hu, Y., De Jong, S., Sluiter, R.: A modeling-based threshold approach to derive change/no change information over vegetation area, Proceedings of the "12 International Conference on Geoinformatics-Geospatial Information Research: Bridging the Pacific and Atlantic". University of Gävle (Sweden), pp. 647-654, 2004.

Huang, J., Wu, P., Zhao, X.: Effects of rainfall intensity, underlying surface and slope gradient on soil infiltration under simulated rainfall experiments. Catena, 104, 93-102, 2013. DOI:10.1016/j.catena.2012.10.013

Jensen, J.R.: Introductory digital image processing: a remote sensing perspective. Prentice-Hall Inc., 1996.

Kendall, M.: Rank correlation methods. 1975.

Liu, B.M., Collick, A.S., Zeleke, G., Adgo, E., Easton, Z.M., Steenhuis, T.S.: Rainfall-discharge relationships for a monsoonal climate in the Ethiopian highlands. Hydrological Processes, 22(7), 1059-1067, 2008.

Lu, D., Mausel, P., Batistella, M., Moran, E.: Comparison of land-cover classification methods in the Brazilian Amazon Basin. Photogrammetric engineering & remote sensing, 70(6), 723-731, 2004.

Mancino, G., Nolè, A., Ripullone, F., Ferrara, A.: Landsat TM imagery and NDVI differencing to detect vegetation change: assessing natural forest expansion in Basilicata, southern Italy. iForest-Biogeosciences and Forestry, 7(2), 75, 2014. DOI:10.3832/ifor0909-007

Mann, H.B.: Nonparametric Tests Against Trend. Econometrica, 13(3), 245-259, 1945.

Marhaento, H., Booij, M.J., Rientjes, T., Hoekstra, A.Y.: Attribution of changes in the water balance of a tropical catchment to land use change using the SWAT model. Hydrological Processes, 31(11), 2029-2040, 2017. DOI:10.1002/hyp.11167

McCartney, M., Alemayehu, T., Easton, Z.M., Awulachew, S.B.: Simulating current and future water resources development in the Blue Nile River Basin. The Nile River Basin: water, agriculture, governance and livelihoods. Routledge-Earthscan, Abingdon, 269-291, 2012.

Mekonnen, D.F., Disse, M.: Analyzing the future climate change of Upper Blue Nile River basin using statistical downscaling techniques. Hydrology and Earth System Sciences, 22(4), 2391-2408, 2018.

Melesse, A., Abtew, W., Dessalegne, T., Wang, X.: Low and high flow analyses and wavelet application for characterization of the Blue Nile River system. Hydrological processes, 24(3), 241, 2009. DOI:10.1002/hyp.7312

Mengistu, D., Bewket, W., Lal, R.: Recent spatiotemporal temperature and rainfall variability and trends over the Upper Blue Nile River Basin, Ethiopia. International Journal of Climatology, 34(7), 2278-2292, 2014. DOI:10.1002/joc.3837

Mockus, V.: National engineering handbook,Section 4:Hydrology, 630, 1964.

Monserud, R.A.: Methods for comparing global vegetation maps. 1990.

Moriasi, D.N., Arnold, J.G., Van Liew, M.W., Bingner, R.L., Harmel, R.D., Veith, T.L.: Model evaluation guidelines for systematic quantification of accuracy in watershed simulations. Trans. Asabe, 50(3), 885-900, 2007.

Neitsch, S., Arnold, J., Kiniry, J.e.a., Srinivasan, R., Williams, J.: Soil and water assessment tool user's manual version 2000. GSWRL report, 202(02-06), 2002.

Neitsch, S.L., Arnold, J.G., Kiniry, J.R., Williams, J.R.: Soil and water assessment tool theoretical documentation version 2009, Texas Water Resources Institute, 2011.

NMA: Annual climate buletien for the year 2013. National Meteorological Agency, Meteorological Data and Climatology Directorate, Addis Ababa, Ethiopia,
5   http://www.ethiomet.gov.et/bulletins/bulletin_viewer/bulletins/348/2013_Annual_Bulletin/en, 2013.

Oki, T., Kanae, S.: Global hydrological cycles and world water resources. science, 313(5790), 1068-1072, 2006. DOI:10.1126/science.1128845

Pettitt, A.: A non-parametric approach to the change-point problem. Applied statistics, 126-135, 1979.

Pignotti, G., Rathjens, H., Cibin, R., Chaubey, I., Crawford, M.: Comparative Analysis of HRU and Grid-Based
10   SWAT Models. Water, 9(4), 272, 2017. DOI:10.3390/w9040272

Polanco, E.I., Fleifle, A., Ludwig, R., Disse, M.: Improving SWAT model performance in the upper Blue Nile Basin using meteorological data integration and subcatchment discretization. Hydrology and Earth System Sciences, 21(9), 4907, 2017. DOI:10.5194/hess-21-4907-2017

Rathjens, H., Oppelt, N.: SWATgrid: An interface for setting up SWAT in a grid-based discretization scheme.
15   Computers & geosciences, 45, 161-167, 2012. DOI:10.1016/j.cageo.2011.11.004

Rathjens, H., Oppelt, N., Bosch, D., Arnold, J.G., Volk, M.: Development of a grid-based version of the SWAT landscape model. Hydrological processes, 29(6), 900-914, 2015. DOI:10.1002/hyp.10197

Rientjes, T., Haile, A., Kebede, E., Mannaerts, C., Habib, E., Steenhuis, T.: Changes in land cover, rainfall and stream flow in Upper Gilgel Abbay catchment, Blue Nile basin-Ethiopia. Hydrology and Earth System
20   Sciences, 15(6), 1979, 2011. DOI:10.5194/hess-15-1979-2011

Seleshi, Y., Zanke, U.: Recent changes in rainfall and rainy days in Ethiopia. International journal of climatology, 24(8), 973-983, 2004. DOI:10.1002/joc.1052

Sen, P.K.: Estimates of the regression coefficient based on Kendall's tau. Journal of the American statistical association, 63(324), 1379-1389, 1968.

25 Setegn, S.G., Srinivasan, R., Dargahi, B.: Hydrological modelling in the Lake Tana Basin, Ethiopia using SWAT model. The Open Hydrology Journal, 2(1), 2008.

Singb, A.: Digital change detection techniques using remotely sensed data. International Journal of Remote Sensing, 10(6), 989L1003, 1989.

Singh, A.: Review article digital change detection techniques using remotely-sensed data. International journal
30   of remote sensing, 10(6), 989-1003, 1989. DOI:10.1080/01431168908903939

Steenhuis, T.S., Winchell, M., Rossing, J., Zollweg, J.A., Walter, M.F.: SCS runoff equation revisited for variable-source runoff areas. Journal of Irrigation and Drainage Engineering, 121(3), 234-238, 1995.

Steenhuis, T.S., Collick, A.S., Easton, Z.M., Leggesse, E.S., Bayabil, H.K., White, E.D., Awulachew, S.B., Adgo, E., Ahmed, A.A.: Predicting discharge and sediment for the Abay (Blue Nile) with a simple model.
35   Hydrological processes, 23(26), 3728-3737, 2009. DOI:10.1002/hyp.7513

Teferi, E., Bewket, W., Uhlenbrook, S., Wenninger, J.: Understanding recent land use and land cover dynamics in the source region of the Upper Blue Nile, Ethiopia: Spatially explicit statistical modeling of systematic transitions. Agriculture, ecosystems & environment, 165, 98-117, 2013. DOI:10.1016/j.agee.2012.11.007

40 Tekleab, S., Mohamed, Y., Uhlenbrook, S., Wenninger, J.: Hydrologic responses to land cover change: the case of Jedeb mesoscale catchment, Abay/Upper Blue Nile basin, Ethiopia. Hydrological Processes, 28(20), 5149-5161, 2014. DOI:10.1002/hyp.9998

Tesemma, Z.K., Mohamed, Y.A., Steenhuis, T.S.: Trends in rainfall and runoff in the Blue Nile Basin: 1964–2003. Hydrological processes, 24(25), 3747-3758, 2010. DOI:10.1002/hyp.7893

Uhlenbrook, S., Mohamed, Y., Gragne, A.: Analyzing catchment behavior through catchment modeling in the Gilgel Abay, upper Blue Nile River basin, Ethiopia. Hydrology and Earth System Sciences, 14(10), 2153-2165, 2010. DOI:10.5194/hess-14-2153-2010

USBR: Land and water resources of the Blue Nile basin, Ethiopia. Main report. United States Bureau of Reclamation, Washington, DC., 1964.

Von Storch, H.: Misuses of Statistical Analysis in Climate Research, Analysis of Climate Variability. Springer, pp. 11-26, 1995.

White, E.D., Easton, Z.M., Fuka, D.R., Collick, A.S., Adgo, E., McCartney, M., Awulachew, S.B., Selassie, Y.G., Steenhuis, T.S.: Development and application of a physically based landscape water balance in the SWAT model. Hydrological Processes, 25(6), 915-925, 2011.

Woldesenbet, T.A., Elagib, N.A., Ribbe, L., Heinrich, J.: Gap filling and homogenization of climatological datasets in the headwater region of the Upper Blue Nile Basin, Ethiopia. International Journal of Climatology, 37(4), 2122-2140, 2017a. DOI:10.1002/joc.4839

Woldesenbet, T.A., Elagib, N.A., Ribbe, L., Heinrich, J.: Hydrological responses to land use/cover changes in the source region of the Upper Blue Nile Basin, Ethiopia. Science of the Total Environment, 575, 724-741, 2017b. DOI:10.1016/j.scitotenv.2016.09.124

Yan, B., Fang, N., Zhang, P., Shi, Z.: Impacts of land use change on watershed streamflow and sediment yield: an assessment using hydrologic modelling and partial least squares regression. Journal of Hydrology, 484, 26-37, 2013. DOI:10.1016/j.jhydrol.2013.01.008

Yin, J., He, F., Xiong, Y.J., Qiu, G.Y.: Effects of land use/land cover and climate changes on surface runoff in a semi-humid and semi-arid transition zone in northwest China. Hydrology and Earth System Sciences, 21(1), 183, 2017a.

Yin, J., He, F., Xiong, Y.J., Qiu, G.Y.: Effects of land use/land cover and climate changes on surface runoff in a semi-humid and semi-arid transition zone in northwest China. Hydrology and Earth System Sciences, 21(1), 183-196, 2017b. DOI:10.5194/hess-21-183-2017

Yue, S., Pilon, P., Phinney, B., Cavadias, G.: The influence of autocorrelation on the ability to detect trend in hydrological series. Hydrological Processes, 16(9), 1807-1829, 2002. DOI:10.1002/hyp.1095

Yue, S., Wang, C.: The Mann-Kendall test modified by effective sample size to detect trend in serially correlated hydrological series. Water Resources Management, 18(3), 201-218, 2004.

Table 1: The UBNRB's areal long term (1971–2010) mean annual and seasonal rainfall and streamflow

Station	Amount				Contribution (%)				
	Kiremit	Belg	Bega	Total	Kiremit	Belg	Bega	Mean	Area (km^2)
Flow (m^{3}s^{-1})	3506.3	300.4	1018.4	4825.1	72.7	6.2	21.1	1608	172254
Flow (BCM)	36.4	3.1	10.6	50.7					
Rainfall (mm)	1070.1	140.8	238.9	1449.8	73.8	9.7	16.5		

Kiremit: long rainy season, Belg: short rainy season, Bega: dry season

Table 2: Data sets of the baseline and altered periods for the SWAT simulation used to analyze the combined and isolated effect of LULC and climate changes on streamflow and water balance components

Model run no.	Combined effect		Isolated LULC change effect		Isolated climate change effect		
	Climate data set	LULC map	Climate data set	LULC map	Climate data set	LULC map	Remark
1	1970s	1973	1970s	1973	1970s	1973	Base period altered
2	1980s	1985	1970s	1985	1980s	1973	Period1 altered
3	1990s	1995	1970s	1995	1990s	1973	Period2 altered
4	2000s	2010	1970s	2010	2000s	1973	Period3

10   Table 3: MK and Pettitt tests for the UBNRB's rainfall and streamflow after TFPW at different time scales

	Stream flow					Rainfall				
	p-value					p-value				
Time scale	After*	Before*	Sen's slope:	Change point	Pettit test	After*	Before*	Sen's slope	Change point	Pettit test
Daily	< 0.0001	< 0.0001	0.013	1987	Increasing	0.387	0.953	0.000	1988	Increasing
Monthly	< 0.0001	0.031	0.378		No change	0.010	0.640	0.009		No change
annually	< 0.0001	0.009	9.619	1995	Increasing	0.006	0.260	1.886		No change
Kiremit	< 0.0001	0.014	20.30		No change	0.010	0.348	1.364		No change
Belg	< 0.0001	0.004	3.593	1985	Increasing	0.822	0.935	0.068		No change
Bega	0.000	0.214	4.832		No change	0.527	0.755	0.169		No change

* Before and after TFPW; p: probability at 5% significance level

Table 4: Summary of the UBNRB's precipitation indices at decadal time series

Indices	1970s	1980s	1990s	2000s
Mean (mm)	4.17	4.05	4.42	4.16
95 percentile (mm)	12.57	12.52	13.66	13.31
99 percentile (mm)	17.34	17.77	19.44	19.65
1-day max (mm)	27.15	25.67	32.24	32.38
R20mm (days)	16	15	30	35
SDII (mm/day)	7.22	7.38	7.66	7.77

SDII is the ratio of total precipitation (mm) to R1mm (days).

Table 5: Confusion (error) matrix for the 2010 land use/cover classification map

LULC class	Water	Forest	Cultivated	Bushes and shrubs	Row total	Producers' accuracy
Water	44	0	0	0	44	100
Forest	1	46	6	8	61	75.4
Cultivated land	2	3	77	15	97	79.4
Bushes and shrubs	1	3	9	73	86	84.9
Column total	48	52	92	86	288	
User's accuracy (%)	91.7	88.5	83.7	84.9		
Over all accuracy(%)	80					
Kappa	0.77					

Table 6: The SWAT model's statistical performance measure values

Period		R^2	NSE	RVE (%)
	Calibration (1973–1977)	0.79	0.74	−3.41
1970s	Validation (1978–1980)	0.84	0.83	7.18
	Calibration (1983–1987)	0.80	0.74	−0.72
1980s	Validation (1988–1990)	0.86	0.82	0.73
	Calibration (1993–1997)	0.91	0.91	1.79
1990s	Validation (1998–2000)	0.87	0.84	−3.56
	Calibration (2003–2007)	0.86	0.86	3.99
2000s	Validation (2008–2010)	0.94	0.92	−7.51

Table 7: SWAT sensitive model parameters and their (final) calibrated values for the four model runs

Parameter	Optimum value			
	1970s	1980s	1990s	2000s
R-CN2	0.88	0.91	0.92	0.9
a-Alpha-BF	0.028	0.028	0.028	0.028
V-GW_REVAPMN	0.7	0.45	0.7	0.34
V-GWQMN	750	750	750	750
V-REVAPMN	550	450	425	550
a-ESCO	−0.85	−0.85	−0.85	−0.85
R-SOL_AWC	6.5	6.5	6.5	6.5

R: value from the SWAT database is multiplied by a given value; V: replace the initial parameter by the given value; a: adding the given value to initial parameter value.

Table 8: Mean annual water-balance-components analysis in the Upper Blue Nile River Basin by considering LULC and climate change over respective periods. All streamflow estimates are for El Diem station.

	Unit	1970s	1980s	1990s	2000s
Precipitation (P)	mm	1428.1	1397.1	1522.2	1462.5
Surface flow (Qs)	mm	112.8	143.4	168.6	141.4
Lateral flow (Ql)	mm	116.8	113.4	125.9	117.6
Base flow (Qb)	mm	47.3	29.6	9.8	64.7
Total water yield (Qt)	mm	276.9	286.3	304.3	323.7
Er=Revap (from shallow aquifer)	mm	269.2	257.2	310.6	241.0
Ea (Ec+Et+Es)	mm	871.6	852.6	904.3	885.0
TAE	mm	1140.8	1109.8	1214.9	1126.0
Recharge (to deep aquifer)	mm	16.7	15.0	16.7	16.3
Change in soil water content	mm	-6.3	-14.0	-13.7	-3.5
Qs/Qt	%	40.7	50.1	55.4	43.7
Qb/Qt	%	17.1	10.3	3.2	20.0
Qt/P	%	19.4	20.5	20.0	22.1
Er (revap)/TAE	%	23.6	23.2	25.6	21.4
Ea/P	%	61.0	61.0	59.4	60.5

where: water yield (Qt) =Qs+ Ql + Qb; Change in soil storage =P-Qs-Ql-Qb-Ea-Revap-Recharge
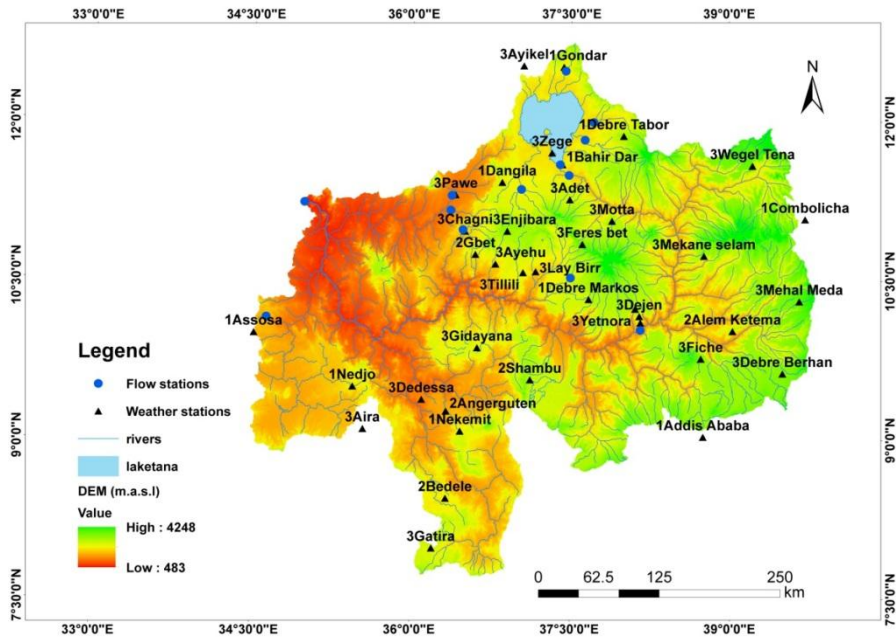
Figure 1: Locations of study area and meteorological and discharge stations, with the Digital Elevation Model (DEM) data as the background (where: 1: Stations used for SWAT model, 2: Stations used for trend analysis, 3: Stations removed from the analysis).
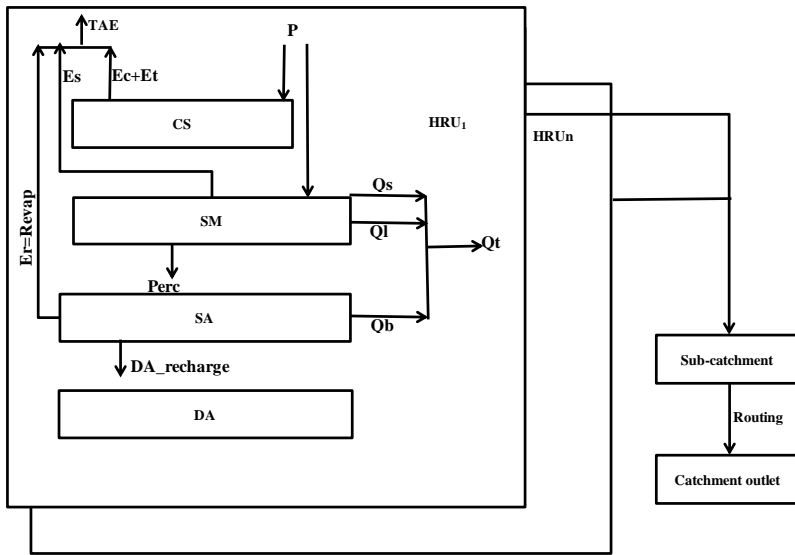
Figure 2: Schematic representation of the SWAT model structure modified from (Marhaento *et al.*, 2017). P is precipitation; CS is canopy storage; TAE is total actual evapotranspiration; Ec is evaopration from the canopy surface; Es is evaporation from the soil surface; Et is transpiration from plants; perc is percolation from the soil storage to shallow aquifer; SM is soil moisture storage; SA is shallow aquifer; Er=Revap is evaporation from the shallow aquifer; Qt is total streamflow; DA is deep aquifer; HRU is hydrological response unit; Qb is base flow; Ql is lateral flow; Qs is surface runoff
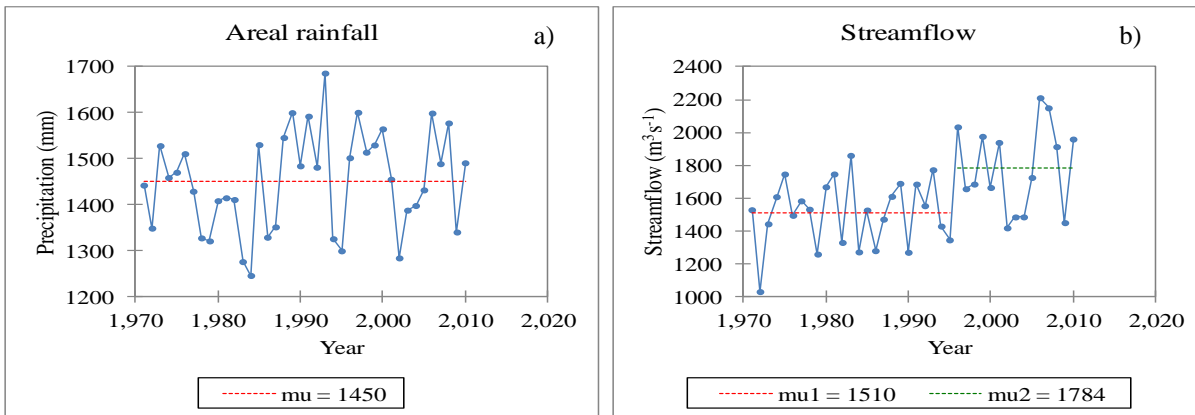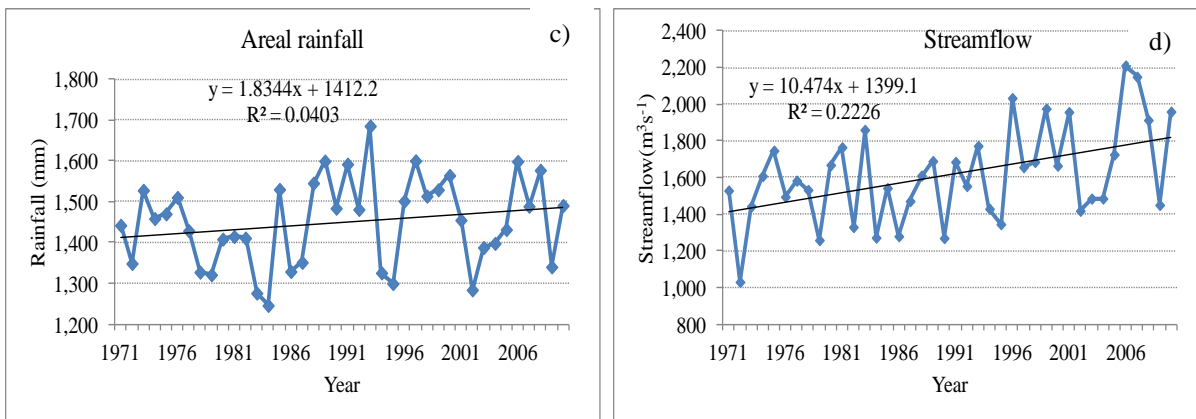
Figure 3: The Pettitt homogeneity test a) annual rainfall, b) annual flow of the UBNRB, c) linear trend of mean annual rainfall and d) linear trend of mean annual streamflow.
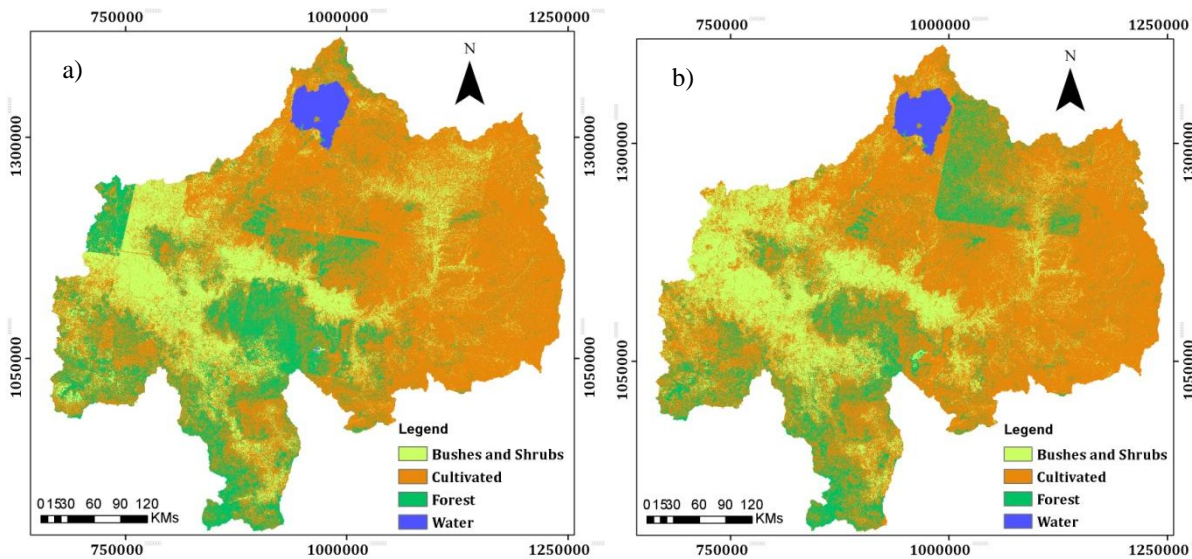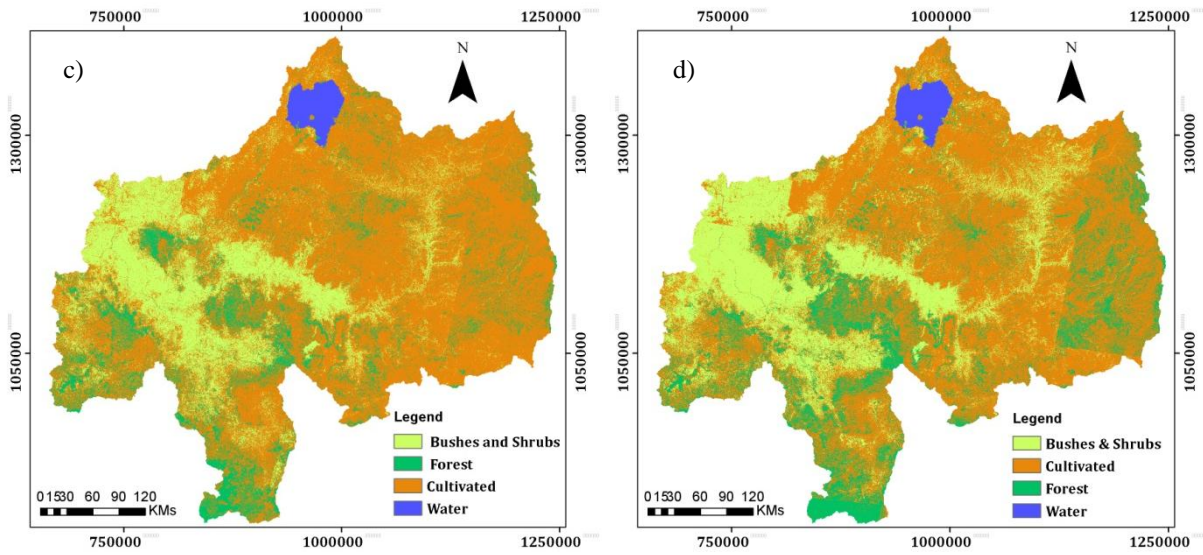
Figure 4: Landcover map of UBNRB derived from Landsat images a) 1973, b) 1985, c) 1995, and d) 2010

10 a)
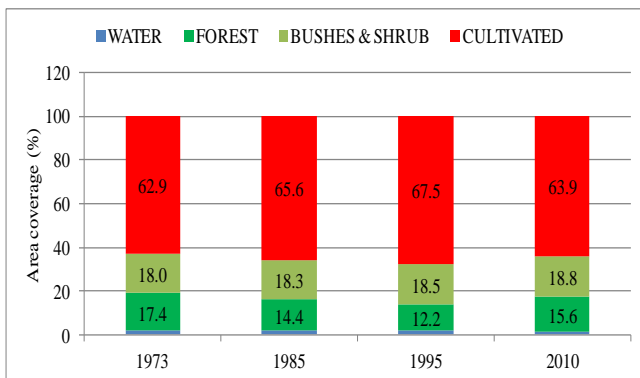
b)
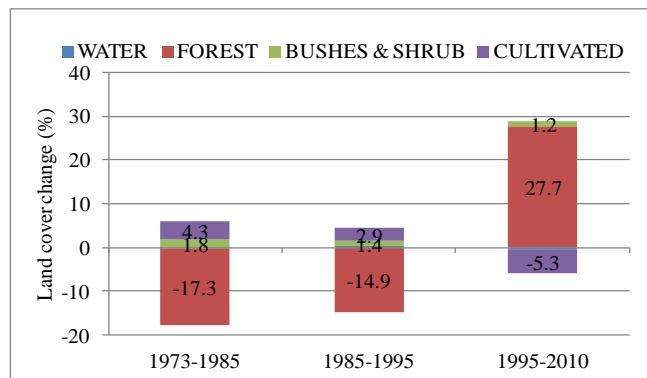
Figure 5: a) LULC composition, b) LULC change in the UBNRB during the period from 1973 to 2010

a)

b)

c)
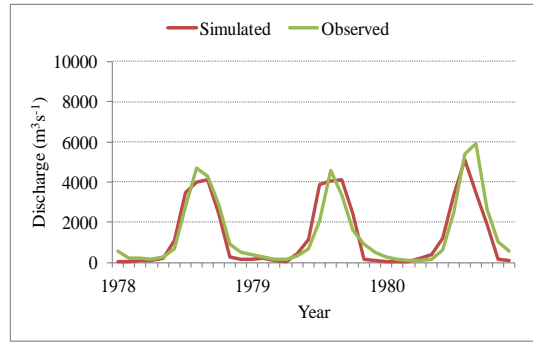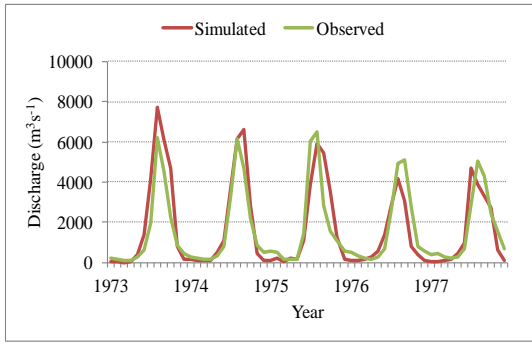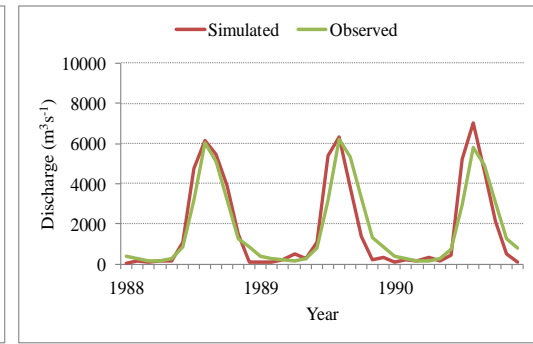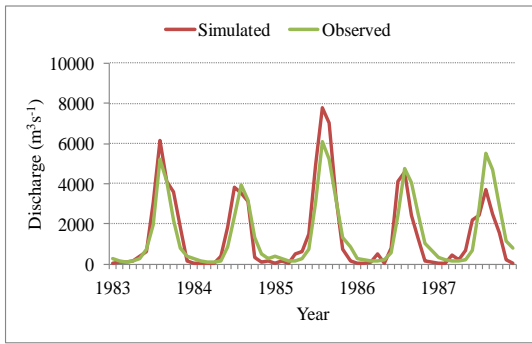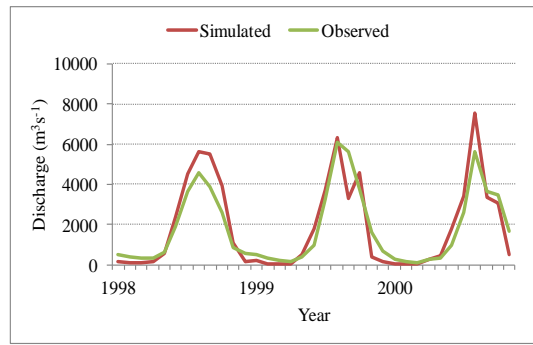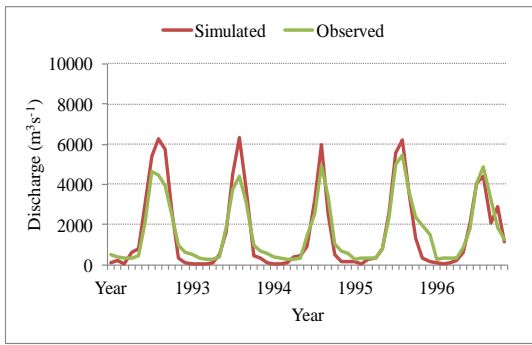
d)
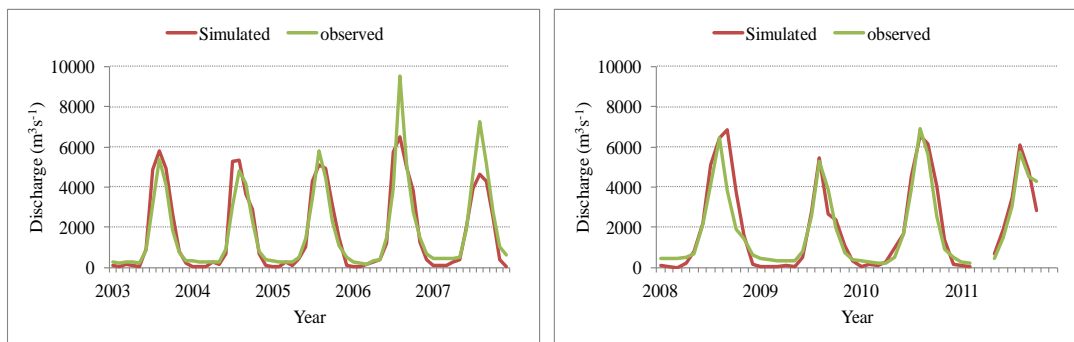
Figure 6: Calibration and validation of the SWAT hydrological model (left and right) respectively at monthly time scale; a) 1970s, b) 1980s, c) 1990s, and d) 2000s
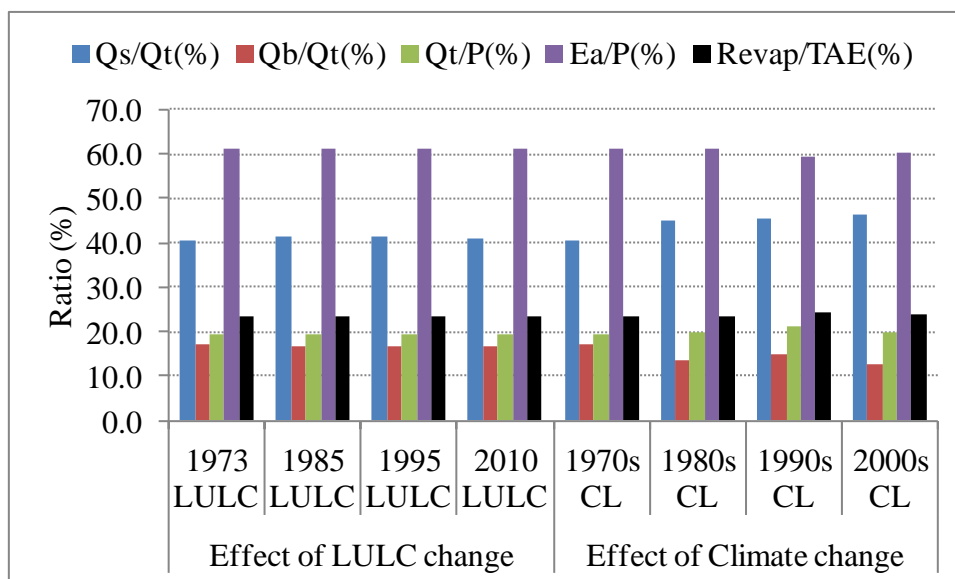
Figure 7: Ratio of water balance component analysis at the El Diem station using an isolated effect (LULC/climate change)